PHYSICAL REVIEW B **88**, 041401(R) (2013)

Spin relaxation times of single-wall carbon nanotubes

W. D. Rice,[1,2] R. T. Weber,[3] P. Nikolaev,[4] S. Arepalli,[5] V. Berka,[6] A.-L. Tsai,[6] and J. Kono[1,2,*]

[1]*Department of Electrical and Computer Engineering, Rice University, Houston, Texas 77005, USA*
[2]*Department of Physics and Astronomy, Rice University, Houston, Texas 77005, USA*
[3]*Bruker BioSpin Corporation, Billerica, Massachusetts 01821, USA*
[4]*Air Force Research Lab, Wright-Patterson Air Force Base, Ohio 45433, USA*
[5]*National Institute of Aerospace, 100 Exploration Way, Hampton, Virginia 23666, USA*
[6]*University of Texas Medical School, Houston, Texas 77005, USA*

(Received 1 May 2013; published 15 July 2013)

We have measured temperature (T)- and power-dependent electron spin resonance in bulk single-wall carbon nanotubes to determine both the spin-lattice and the spin-spin relaxation times, T_1 and T_2. We observe that T_1^{-1} increases linearly with T from 4 K to 100 K, whereas T_2^{-1} *decreases* by over a factor of two when T is increased from 3 K to 300 K. We interpret the $T_1^{-1} \propto T$ trend as spin-lattice relaxation via interaction with conduction electrons (Korringa law) and the decreasing T dependence of T_2^{-1} as motional narrowing. By analyzing the latter, we find the spin hopping frequency to be 285 GHz. Last, we show that the Dysonian line shape asymmetry follows a three-dimensional variable-range hopping behavior from 3 K to 20 K; from this scaling relation, we extract a localization length of the hopping spins to be ∼100 nm.

DOI: 10.1103/PhysRevB.88.041401 PACS number(s): 76.30.−v, 72.20.Ee, 73.63.Fg

Understanding spin dynamics is key to a broad range of modern problems in condensed-matter physics[1–6] and applied sciences.[7,8] Spin transport is a sensitive probe of many-body correlations as well as an indispensable process in spintronic devices. Confined spins, particularly those in one dimension (1D), are predicted to show strong correlations[2,4–6,9] and long coherence times.[3] Single-wall carbon nanotubes (SWCNTs) are ideal materials for studying 1D spin physics due to their long mean free paths and relatively weak spin-orbit coupling.[10] Exotic spin properties in metallic SWCNTs at low temperatures and high magnetic fields have been predicted, including the appearance of a peak splitting in the spin energy density spectrum, which can be used to probe spin-charge separation in Luttinger-liquid theory.[4–6]

One method for studying spin dynamics is electron spin resonance (ESR), which can provide information on spin-orbit coupling, phase relaxation time, spin susceptibility, and spin diffusion. Many ESR studies of SWCNTs have been performed over the past decade.[5,6,11–22] Unfortunately, substantial conflicts have emerged in the literature, such as the temperature (T) dependence of the spin susceptibility[12,15,18,22] and whether the ESR is caused by SWCNT defects[11,15,17,21,22] or is intrinsic to nanotubes.[12,13,16,18–20] Because of these divergent empirical observations of nanotube ESR, there is only scant experimental data on electron spin-lattice relaxation times in SWCNTs, which limits our understanding of nanotube spin dynamics.

Here, we present a detailed study of the T dependence of both the spin-lattice (T_1) and spin-spin (T_2) relaxation times of paramagnetic electron spins in SWCNTs. From the T dependence of T_1, we find that the spin-lattice relaxation rate, T_1^{-1}, is proportional to T. This trend is consistent with the notion that the probed spins relax through interaction with conduction electrons that are present in metallic SWCNTs in the sample. Additionally, we find that the dephasing rate, T_2^{-1}, becomes smaller as T is increased, which is a hallmark of the phenomenon of motional narrowing.[23,24] This spin mobility accounts for the Dysonian line shape[25] seen throughout the full T range examined. The Dysonian line-shape asymmetry parameter, α, which is proportional to the conductivity of the probed spins, is shown to follow the 3D variable-range hopping (VRH) trend at low T.

Our sample consisted of acid-purified laser-oven SWCNTs in powder form, which we prepared using a comprehensive nanotube compaction and annealing procedure.[22] After thermal annealing, the 630-μg (0.24 g/cm^3) SWCNT sample was submerged in mineral oil under helium gas in a sealed quartz tube. To precisely know the value of the perturbing ac magnetic field amplitude, H_1, at a given microwave power, we calibrated the dual-mode cavity (Bruker ER4116DM resonator) with a α-γ-bisdiphenylene-β-phenylallyl (BDPA) complex mixed 1:1 with benzene. H_1 is related to the microwave power, P, at a given cavity Q by $H_1 = \alpha_C\sqrt{(Q/Q_0)P}$, where α_C is the cavity conversion factor and Q_0 is the loaded-cavity quality factor during calibration.[26] To obtain α_C, we measured the T_1 of the BDPA sample using inversion recovery[27] to be $T_1 = 132$ ns. We then performed ESR power saturation spectroscopy on the BDPA calibration sample at $Q_0 = 5100$ and observed that the absorption versus microwave power saturated at 65 mW. Using these data in conjunction with the T_1 and T_2 (=112 ns) values for our BDPA sample, we established $\alpha_C = 1.83\ \mathrm{G}/\sqrt{\mathrm{W}}$.

ESR spectra were taken as a function of T from 3.4 K to 300 K in the X-band (9.6-GHz) region. ESR data below 125 K were taken on a Bruker EMX spectrometer using the TE_{102} mode in a dual-mode cavity (Bruker ER4116DM); for $T \geqslant$ 125 K, we used a single-mode resonator (Bruker ER4119HS). For the lower T regime, detailed ESR scans were performed with a P of 200 μW ($H_1 \sim 1.62 \times 10^{-2}$ G), while for $T \geqslant$ 125 K, P of 1 mW ($H_1 \sim 7.31 \times 10^{-2}$ G) was used. At certain T values below 125 K, we varied P from 6.3 μW to 200 mW in steps of 3 dB at an observed Q of 2000 to examine how the relative spin susceptibility changed with H_1, as detailed by Portis.[28]

As seen in Fig. 1(a), a broad ferromagnetic resonance (FMR) dominates the spectrum, which we attribute to nickel and cobalt catalyst particles remaining in the sample.[18] A careful study of the line shape was performed by closely

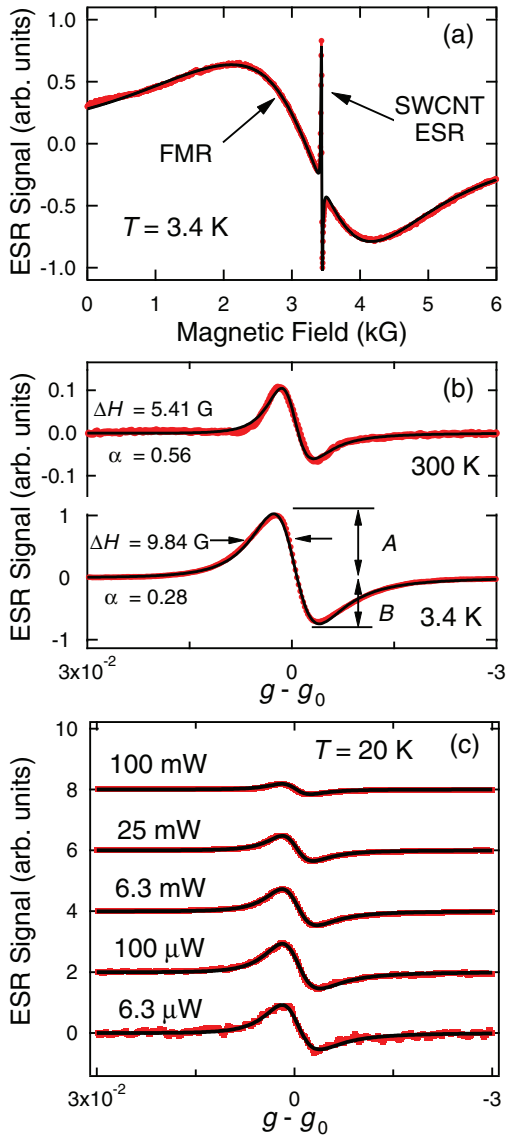

FIG. 1. (Color online) (a) A raw ESR spectrum taken at 3.4 K across a 6-kG applied field range. A prominent ESR peak can be seen on top of a large ferromagnetic resonance (FMR) background. A Dysonian and two Lorentzian line shapes can be used to fully fit the data (black line). (b) Background-subtracted ESR scans with Dysonian line-shape fits for the highest (300 K) and lowest temperatures (3.4 K). The Dysonian amplitude and linewidth is clearly much smaller at 300 K than at 3.4 K. (c) Comparison of ESR traces at 20 K for different microwave powers, showing clear absorption saturation at high powers. The background was subtracted as in (b), and the spectra are intentionally offset vertically.

scanning the applied dc magnetic field, H_0, around the ESR peak. Both the linewidth and peak-to-peak amplitude become larger as T is decreased, while the line-center position (g factor, or simply, g_0) shows little T dependence. The ESR line is asymmetric, as seen in Fig. 1(b), having what is often referred to as a Dysonian line shape,[25] indicating movement of the electrons in and out of the H_1 perturbing magnetic field. Figure 1(c) shows five traces at 20 K at different microwave powers, spanning more than four orders of magnitude. As P is increased, the relative ESR signal begins to decrease, as evidenced by the reduction of the signal, normalized for P, as P is increased from 6.3 μW to 100 mW.

To gain further quantitative understanding, we numerically fit each ESR spectrum. The FMR background was fit by a combination of two large-linewidth (~1000 G) Lorentzians. The ESR feature was fit using the weak form of the Dysonian line shape[18,29]

$$\frac{d\chi}{dH_0} = A\chi_g\left(\frac{\cos\varphi}{\Delta H_0^2}\right)\frac{-2y+(1-y^2)\tan\varphi}{(1+y^2)^2}, \qquad (1)$$

where A is a coefficient accounting for experimental factors, χ_g is the mass spin susceptibility, $y = \frac{H_0-H_r}{\Delta H_0}$, H_r is the resonance field, ΔH_0 is the half width and is equal to $\frac{1}{\gamma T_2}$, with $\gamma = \frac{g\mu_B}{\hbar}$, and μ_B the Bohr magneton. The weak form of Dysonian can be used here because the conductivity and diffusion of the electrons in the SWCNT powder are both low as compared to a traditional metal. Nevertheless, unlike traditional magnetic resonance where the signal entirely depends on the imaginary part of the ac spin susceptibility, χ'', the Dysonian line shape is also influenced by the real component, χ'. Taking the ac susceptibility, χ, to be

$$\chi = \chi''\cos\varphi + \chi'\sin\varphi, \qquad (2)$$

we define $\alpha \equiv \tan\varphi$, which is a dimensionless measure of the relative contribution of the real part (=0 for traditional, fixed spin ESR). This parameter is also a measure of the asymmetry of the line shape, and $A/B \approx 1+\alpha$ when $\alpha \ll 1$, where A and B are defined in Fig. 1(b); additionally, it can be related to the electrical conductivity of the probed spins, σ_{spin}, as $\alpha \propto \sigma_{spin}$.[29]

From the numerical fitting, we extracted T_2, α, g_0, and $A\chi_g$ for each curve as a function of P and T. Since we are in the homogeneous broadening regime, as indicated by the Lorentzian-like line shape fitting for all curves, we can use the two-level model of χ'':

$$\chi''(P) = \chi_g\frac{\omega_r T_2}{1+(\omega_0-\omega_r)^2T_2^2+\gamma^2H_1^2T_1T_2}, \qquad (3)$$

where $H_1 = \alpha_C\sqrt{(Q/Q_0)P}$, $\hbar\omega_0 = g\mu_B H_0$, and ω_r is the center of the resonance. At small values of P, we can ignore the last term in the denominator, since it will contribute negligibly to the line shape. However, as P becomes larger, this saturation term becomes increasingly important, leading to a decrease in χ''. By taking the ratio of $\chi''(P)$ to $\chi''(P\to 0)$ the effect of this saturation term can be clearly delineated:[28,30]

$$\frac{\chi''(P)}{\chi''(0)} = \frac{1}{1+\gamma^2H_1^2T_1T_2}. \qquad (4)$$

To reduce the experimental errors for the weak signals when P is of the order of 10^{-5} W, we averaged the values of $A\chi_g$ (after normalizing for P), T_2, and γ for spectra taken when P was in the linear regime. The ratio of $\chi''(P)/\chi''(0)$ is equivalent to the ratio of $A\chi_g(P)/A\chi_g(0)$, as long as the ESR is not inhomogeneous broadened with increasing P.

A typical plot of $\chi''(P)/\chi''(0)$ versus P at 20 K is given in Fig. 2(a). For other T's, Eq. (4) also fits well, although minor sample heating effects at the highest powers are seen when $T <$ 10 K. From the power saturation fitting, along with the knowledge of T_2 and γ, we can extract T_1 for each T. T_1 is found to monotonically increase as T decreases [Fig. 2(b)]: When T

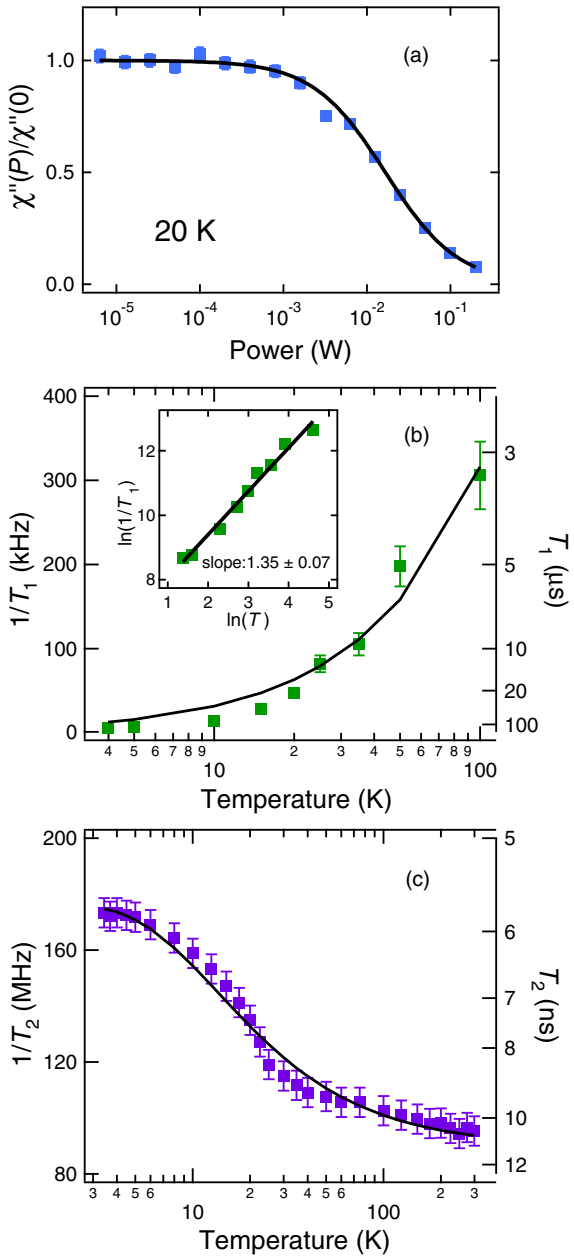

FIG. 2. (Color online) (a) Normalized spin susceptibility versus the microwave power, P, at 20 K. The black line shows the fit of Eq. (4) to the data. (b) The T dependence of the spin-lattice relaxation rate, $1/T_1$. The fit of $1/T_1 = CT$ is shown by the black line. (Inset) A plot of $\ln(1/T_1)$ versus $\ln(T)$ shows that data follow a linear relation over the entire measured T range. (c) The T-dependent spin-spin relaxation rate, $1/T_2$, and the fit of Eq. (6) to the data (black line).

is lowered from 100 K to 4 K, T_1 rises from 3.3 to 172 μs, in agreement with written claims by Clewett *et al.*[31] and the measurements done below 30 K by Musso and co-workers.[17]

To better understand the spin-lattice relaxation mechanism, we plotted $\ln(1/T_1)$ against $\ln(T)$ [inset of Fig. 2(b)] and observe a nearly linear scaling: $T_1^{-1} \propto T^{1.35\pm0.07}$. This T dependence closely matches both the Korringa law and direct one-phonon relaxation mechanisms, which go as $T_1^{-1} = CT$, where C is a proportionality constant. As Fig. 2(b) shows, the one-variable linear fit follows the general trend of the data well; from this fit, we extract the value of C to be $(2.8 \pm 0.4) \times 10^3$ s^{-1} K^{-1}.

This T-linear behavior of T_1^{-1} is consistent with spin-lattice relaxation via interaction with either conduction electrons (Korringa law) or phonons.[32] Since the g-factor difference from the free electron value ($\Delta g = g - 2.0023$) suggests small spin-orbit coupling in our system,[22] direct spin-phonon interactions are minimal. In addition, we used a nonenriched SWCNT system, where metallic nanotubes are present. Thus, we believe that a Korringa law spin-lattice relaxation process is the most likely explanation of the $T_1^{-1} \propto T$ trend. In this scenario, the probed spins are exchange-coupled to delocalized conduction electrons within k_BT of the Fermi level. Similar conclusions about the spin relaxation were reached in $C_{59}N$-C_{60} heterodimers in an ensemble of nonenriched SWCNTs.[33,34] However, Musso *et al.* also saw a linear relationship between T_1^{-1} and T in nonenriched SWCNTs over a limited range (4 K to 30 K) but interpreted it in terms of direct phonon relaxation.[17]

We also obtained T_2^{-1} from the fitting of the ESR spectra in the linear regime of H_1. Unlike previous studies of ESR in nanotubes, T_2^{-1} changes substantially with T. As Fig. 2(c) shows, as T is increased from 3.4 K, T_2^{-1} rapidly *decreases* until ~25 K, whereupon the dephasing rate begins to decrease more slowly up to 300 K. This decrease of the ESR linewidth with increasing T is consistent with the phenomenon of motional narrowing,[23,24] which occurs because the dephasing time of the spins can change as their translational energy is altered. At high T, the spins move rapidly, allowing for less time around dephasing centers, thus reducing the interaction between the probed spins and the dephasing centers. This decreased interaction gives a longer spin dephasing time (T_2), which in turn narrows the line shape; conversely, at low T, the spins are moving more slowly, which broadens the line.

To understand the observation of motional narrowing more quantitatively, we start with a generalized narrowing model,[35,36]

$$T_2^{-1} \simeq \frac{\gamma \Delta H_p^2}{\Delta H_e}, \tag{5}$$

where ΔH_p is the amplitude of the perturbations and ΔH_e describes the rate of spin motion. Equation (5) was originally derived to describe exchange narrowing or motional narrowing from spin diffusion. However, spin diffusion can be described in terms of phonon-activated hopping with a probability, $p_{\rm hop}$, that is proportional to $\exp(-2R/\xi - \Delta E/k_BT)$.[37–39] Here, R is the hopping distance, ξ is the localization length, ΔE is the average spacing between energy levels, and k_B is the Boltzmann constant. Combining this hopping conduction with Eq. (5) and adding an offset, $(T_2^0)^{-1}$, gives[40,41]

$$T_2^{-1} = \left(T_2^0\right)^{-1} + \gamma \frac{A}{\Delta E \times \left[1 + \coth\left(\frac{\Delta E}{2k_BT}\right)\right]}, \tag{6}$$

where T_2^0 is the high-T ("metallic") asymptotic limit of the spin dephasing time and A is independent of T. As Fig. 2(c) shows, Eq. (6) fits very well to the observed linewidth. We find A to be 11.6 ± 0.8 meV G and a T_2^0 spin dephasing time of 11.1 ns. The activation energy, ΔE, is 1.18 ± 0.09 meV (13.7 K or

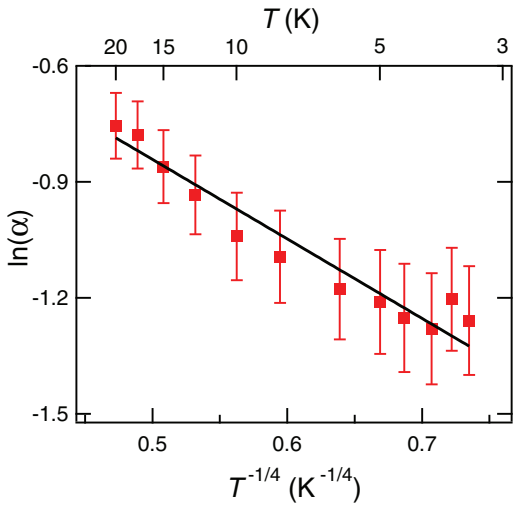

FIG. 3. (Color online) The natural log of the asymmetry Dysonian parameter, α, plotted against the fourth root of inverse temperature. The trend of $\ln(\alpha)$ follows a 3D VRH behavior, as given by the best-fit line in black.

285 GHz). From the value of ΔE, we estimate how much time (on average) each spin spends at each hopping location, $\tau = \frac{\hbar}{\Delta E} = 558$ fs.[42] If we phenomenologically take $T_2 = n\tau$, where n is the number of jumps before phase coherence is lost, then we can estimate n to be on the order of 10^4 hops, where we have taken T_2 to be $\sim$10 ns.

To gain deeper insight into the spin hopping mechanism, we examined the asymmetry Dysonian line shape parameter, α, which is proportional to the conductance of the probed spins. In particular, we were interested to see if α followed a VRH behavior at low T, which is mathematically given as[38,39]

$$\alpha = \alpha_0 \times \exp\left[-\left(\frac{T_0}{T}\right)^{\frac{1}{1+d}}\right], \tag{7}$$

where T_0 is the characteristic temperature and d is the dimensionality of the system. As Fig. 3 shows, $\ln(\alpha)$ follows a linear trend with $T^{-\frac{1}{4}}$, indicating that the spins follow a 3D VRH from 3.4 K to 20 K. From our fit, T_0 is 17.9 ± 5.5 K and α_0 is 1.20. The asymptotic limit of the α parameter, α_0, approaches 1 as $T \to 0$, since the asymmetry of the ESR signal is caused by thermally activated hopping: As the phonon density decreases, so does the line-shape asymmetry. The localization length, ξ, of the electronic wave function can be found from T_0 (Ref. 39),

$$\xi = \left[\frac{18.1}{k_B T_0 D(E_F)}\right]^{1/3}, \tag{8}$$

where $D(E_F)$ is the density of states around the Fermi energy, E_F. We can estimate $D(E_F)$ by treating the defect density of states as having an energy separation that can be roughly estimated by ΔE. Thus, $D(E_F) \approx \frac{N(E_F)}{\Delta E} \sim 10^{19}$ states/cm^3 eV, where we are utilizing the spin density extracted from the Curie constant, $N(E_F) = 1.14 \times 10^{16}$ spins/cm^3 obtained in our earlier work.[22] From Eq. (8), we estimate ξ to be $\sim$100 nm, similar to previous measurements of defect-induced localization lengths in SWCNTs.[43] The spacing of defects, R_d, can be estimated by $(\frac{4\pi}{3}N)^{-1/3}$, or $\sim$28 nm. A $d = 3$ VRH behavior is expected in this wave-function-overlap regime, since $R_d < \xi$ (Ref. 38). Exchange effects may also be important, but a thorough defect concentration dependence is needed to investigate this avenue more fully.

It is important to note that, given the difficulty in extracting α, the $T^{-1/4}$ trend that we are observing can be considered robust. We also performed traditional conductance measurements on a similarly prepared sample, and although the conductance clearly showed 3D VRH behavior, we believe that our ESR and four-point probe conductivity measurements are probing different species, since the hopping parameters do not agree and the high-T trends are different.

Although it is clear that the ESR signal arises from nanotubes, its microscopic origin is not certain. Previously, we advocated that n-type defects are essential for the SWCNT ESR, a conclusion based on the observation that ESR signal strongly depends on the presence of molecular oxygen (a p-type acceptor), which we attribute to a compensation mechanism.[22] This hypothesis is consistent with the data we present here. Localized spins that couple via the exchange interaction to conduction electrons would show a $T_1^{-1} \propto T$ scaling behavior. ESR-active defect states would explain the localized, phonon-assisted hopping of the spins and the motional narrowing of T_2; this type of line narrowing was observed in doped semiconductors. Furthermore, if we take the spin susceptibility value, $\chi_g = 1.11 \pm 0.04 \times 10^{-7}$ emu K/g and calculate the number of spins per unit cell, assuming an idealized 1-μm-long, (10,10) nanotube (similar to our average diameter), we find that there are 1.4×10^{-4} ESR-active spins per unit cell, a substantial deviation from the $\approx$1 spin/unit cell expected for an intrinsic SWCNT response. If this ESR-active defect hypothesis is correct, the wide variety of prior SWCNT ESR results may be due to the different defect concentrations, which would change the T dependencies of T_1, T_2, α, and χ_g.

In summary, we have performed temperature- and power-dependent ESR on an ensemble of SWCNTs. We find $T_1^{-1} \propto T$ from 4 to 100 K, which we interpret as Korringa spin-lattice relaxation. Furthermore, we observe that T_2 undergoes motional narrowing as T is increased from 3.4 K to 300 K. The Dysonian asymmetry parameter, α, follows a $T^{-1/4}$ trend at $T \leqslant 20$ K, which strongly suggests a 3D VRH spin transport at low T. From the extracted parameters, we estimate the spin localization length to be $\sim$100 nm. These results provide significant new insights into spin relaxation dynamics in SWCNTs.

This work was supported by the DOE/BES (Grant No. DEFG02-06ER46308), the NSF (Grant Nos. OISE-0530220 and OISE-0968405), the Robert A. Welch Foundation (Grant No. C-1509), the Air Force Research Laboratories (Grant No. FA8650-05-D-5807), the W. M. Keck Program in Quantum Materials at Rice University, the Korean Ministry of Education, Science, and Technology under the World Class University Program (Grant No. R31-2008-10029), and the NIH National Heart, Lung, and Blood Institute (Grant No. HL095820). We thank Q. Si, A. Imambekov, and R. Hauge for useful discussions.

*Corresponding author: kono@rice.edu

[1]Q. Si, Phys. Rev. Lett. **78**, 1767 (1997); **81**, 3191 (1998).
[2]L. Balents and R. Egger, Phys. Rev. Lett. **85**, 3464 (2000); Phys. Rev. B **64**, 035310 (2001).
[3]A. A. Kiselev and K. W. Kim, Phys. Rev. B **61**, 13115 (2000).
[4]S. Rabello and Q. Si, Europhys. Lett. **60**, 882 (2002).
[5]A. De Martino, R. Egger, K. Hallberg, and C. A. Balseiro, Phys. Rev. Lett. **88**, 206402 (2002).
[6]B. Dóra, M. Gulácsi, J. Koltai, V. Zólyomi, J. Kürti, and F. Simon, Phys. Rev. Lett. **101**, 106408 (2008).
[7]D. P. DiVincenzo, Science **270**, 255 (1995).
[8]S. A. Wolf, D. D. Awschalom, R. A. Buhrman, J. M. Daughton, S. von Molnar, M. L. Roukes, A. Y. Chtchelkanova, and D. M. Treger, Science **294**, 1488 (2001).
[9]T. Giamarchi, *Quantum Physics in One Dimension* (Oxford University Press, Oxford, 2004).
[10]T. Ando, J. Phys. Soc. Jpn. **69**, 1757 (2000).
[11]M. Kosaka, T. W. Ebbesen, H. Hiura, and K. Tanigaki, Chem. Phys. Lett. **233**, 47 (1995).
[12]P. Petit, E. Jouguelet, J. E. Fischer, A. G. Rinzler, and R. E. Smalley, Phys. Rev. B **56**, 9275 (1997).
[13]A. S. Claye, N. M. Nemes, A. Jánossy, and J. E. Fischer, Phys. Rev. B **62**, R4845 (2000).
[14]K. Shen, D. L. Tierney, and T. Peitraß, Phys. Rev. B **68**, 165418 (2003).
[15]J.-P. Salvetat, T. Fehér, C. L'Huillier, F. Beuneu, and L. Forró, Phys. Rev. B **72**, 075440 (2005).
[16]B. Náfrádi, N. M. Nemes, T. Fehér, L. Forró, Y. Kim, J. E. Fischer, D. E. Luzzi, F. Simon, and H. Kuzmany, Phys. Status Solidi B **243**, 3106 (2006).
[17]S. Musso, S. Porro, M. Rovere, A. Tagliaferro, E. Laurenti, M. Mann, K. B. K. Teo, and W. I. Milne, Diamond Relat. Mater. **15**, 1085 (2006).
[18]V. Likodimos, S. Glenis, N. Guskos, and C. L. Lin, Phys. Rev. B **76**, 075420 (2007).
[19]B. Corzilius, K.-P. Dinse, K. Hata, M. Haluška, V. Skákalová, and S. Roth, Phys. Status Solidi B **245**, 2251 (2008).
[20]J. Kombarakkaran and T. Pietraß, Chem. Phys. Lett. **452**, 152 (2008).
[21]N. Ferrer-Anglada, A. A. Monge, and S. Roth, Phys. Status Solidi B **247**, 2823 (2010).
[22]W. D. Rice, R. T. Weber, A. D. Leonard, J. M. Tour, P. Nikolaev, S. Arepalli, V. Berka, A.-L. Tsai, and J. Kono, ACS Nano **6**, 2165 (2012).
[23]N. Bloembergen, E. M. Purcell, and R. V. Pound, Phys. Rev. **73**, 679 (1948).
[24]R. Kubo and K. Tomita, J. Phys. Soc. Jpn. **9**, 888 (1954).
[25]F. J. Dyson, Phys. Rev. **98**, 349 (1955).
[26]C. P. Poole, *Electron Spin Resonance: A Comprehensive Treatise of Experimental Techniques*, 1st ed. (Wiley, New York, 1983).
[27]D. L. Rabenstein, T. Nakashima, and G. Bigam, J. Magn. Reson. **34**, 669 (1979).
[28]A. M. Portis, Phys. Rev. **91**, 1071 (1953).
[29]V. Sitaram, A. Sharma, S. V. Bhat, K. Mizoguchi, and R. Menon, Phys. Rev. B **72**, 035209 (2005).
[30]S. Tóth, D. Quintavalle, B. Náfrádi, L. Korecz, L. Forró, and F. Simon, Phys. Rev. B **77**, 214409 (2008).
[31]C. F. M. Clewett, P. Li, and T. Pietraß, J. Phys. Chem. C **111**, 6263 (2007).
[32]H. Kuzmany, *Solid-State Spectroscopy: An Introduction* (Springer-Verlag, Heidelberg, Germany, 1998).
[33]F. Simon, H. Kuzmany, B. Náfrádi, T. Fehér, L. Forró, F. Fülöp, A. Jánossy, L. Korecz, A. Rockenbaur, F. Hauke *et al.*, Phys. Rev. Lett. **97**, 136801 (2006).
[34]F. Simon, D. Quintavalle, A. Jánossy, B. Náfrádi, L. Forró, H. Kuzmany, F. Hauke, A. Hirsch, J. Mende, and M. Mehring, Phys. Status Solidi B **244**, 3885 (2007).
[35]P. W. Anderson and P. R. Weiss, Rev. Mod. Phys. **25**, 269 (1953).
[36]P. W. Anderson, J. Phys. Soc. Jpn. **9**, 316 (1954).
[37]A. Miller and E. Abrahams, Phys. Rev. **120**, 745 (1960).
[38]N. Mott, *Conduction in Non-Crystalline Materials*, 2nd ed. (Oxford University Press, New York, 1993).
[39]H. Kamimura and H. Aoki, *The Physics of Interacting Electrons in Disordered Systems*, 1st ed. (Clarendon Press, New York, 1989).
[40]D. K. Wilson, Phys. Rev. **134**, A265 (1964).
[41]K. Morigaki and T. Mitsuma, J. Phys. Soc. Jpn. **20**, 62 (1965).
[42]C. Kittel, *Introduction to Solid State Physics*, 7th ed. (Wiley & Sons, New York, 1996).
[43]C. Gómez-Navarro, P. J. D. Pablo, J. Gómez-Herrero, B. Biel, F. J. Garcia-Vidal, A. Rubio, and F. Flores, Nat. Mater. **4**, 534 (2005).